Holistic scan optimization of nacelle-mounted lidars for inflow and wake characterization at the RAAW and AWAKEN field campaigns

Stefano Letizia[1], Nicola Bodini[1], Peter Brugger[2], Andrew Scholbrock[1], Nicholas Hamilton[1], Fernando Porté-Agel[2], Paula Doubrawa[1] and Patrick Moriarty[1]

[1] National Renewable Energy Laboratory, Golden, CO 80401, USA
[2] École Polytechnique Fédérale de Lausanne, Lausanne, CH

E-mail: stefano.letizia@nrel.gov

Abstract. In this article, we provide a methodological framework for designing the scanning strategies of nacelle-mounted scanning lidars for wind energy field experiments, and apply it at two major experimental field campaigns. For the Rotor Aerodynamics, Aeroelastics, and Wake project (RAAW), we leverage two scanning lidars on one turbine to characterize the incoming turbulence and the turbine wake. For the American WAKE experimeNt (AWAKEN), we use four scanning lidars on top of four turbines in a large wind power plant to investigate both individual wakes and wind-plant-scale flow features.

1. Introduction

It is well-known that wind turbines affect the local flow conditions, creating wakes that impact the power production of nearby generators [1]. The prediction of the impact of wake interaction on the energy capture is additionally complicated by the fact that the length and magnitude of a wind plant wake are variable, depending on the inflow wind speed, wind direction, atmospheric stratification, wind shear, wind veer, and wind turbine operating regime [2]. Furthermore, the growth of the wind energy industry is forcing investors to install turbines in increasingly unfavorable sites, such as close to preexisting wind power plants. Wind plant wakes can persist for several kilometers downwind of wind turbines and cause significant economic impacts on the downwind power plant [3].

Another macroscopic effect that is gaining interest from the scientific community is blockage (i.e., the reduction of the incoming wind by the aggregated effect of the pressure fields induced by turbine thrust). Although it can cause significant energy losses [4], its quantification and detection is exceptionally difficult because it is easily overshadowed by experimental and statistical uncertainties [5, 6].

In light of the challenges described earlier, the need for comprehensive, quality-controlled field experimental wind data arises as a number-one priority to advance the current wind power plant models and engineering tools. In this context, remote sensing represents a flexible and powerful tool for characterizing the wind flow. Specifically, scanning lidar technology allows the user to direct the beam in selected directions and control spatial and angular resolutions, thus

expanding the range of the detectable volumes compared to traditional anemometers [7], despite a lower temporal frequency compared to sonic anemometers.

Scanning lidars have been widely used for wind energy in the last decade. The majority of the studies focused on the characterization of single wind turbine wakes [8], wind resource assessment [9], inflow detection [10], and blockage [5]. The scanning lidar's capabilities require user input to define the scan patterns used, and thus the quantities and scales observed. The body of work applying lidar to wind energy has resulted in a striking variety of scanning strategies to detect quantities of interest, whereas general guidelines are practically missing. In this study, we propose a rigorous procedure to determine the optimal experimental setup for nacelle-mounted scanning lidars to characterize both inflow and wind turbine wakes at two field campaigns currently taking place in the United States—the Rotor Aerodynamics, Aeroelastics, and Wake project (RAAW) and American WAKE experimeNt (AWAKEN) field campaigns.

2. Methodology

Our proposed methodology for identifying the optimal scanning strategy for a generic field campaign using scanning lidars builds upon the LiDAR Statistical Barnes Objective Analysis (LiSBOA) framework [11, 12], which was conceived to optimally conduct and objectively analyze stationary lidar measurements, which are here extended to include the deployment of multiple lidars and characterization of time-varying turbulent fields. Figure 1 summarizes the overall workflow, whereas the next paragraphs discuss the details of each step.

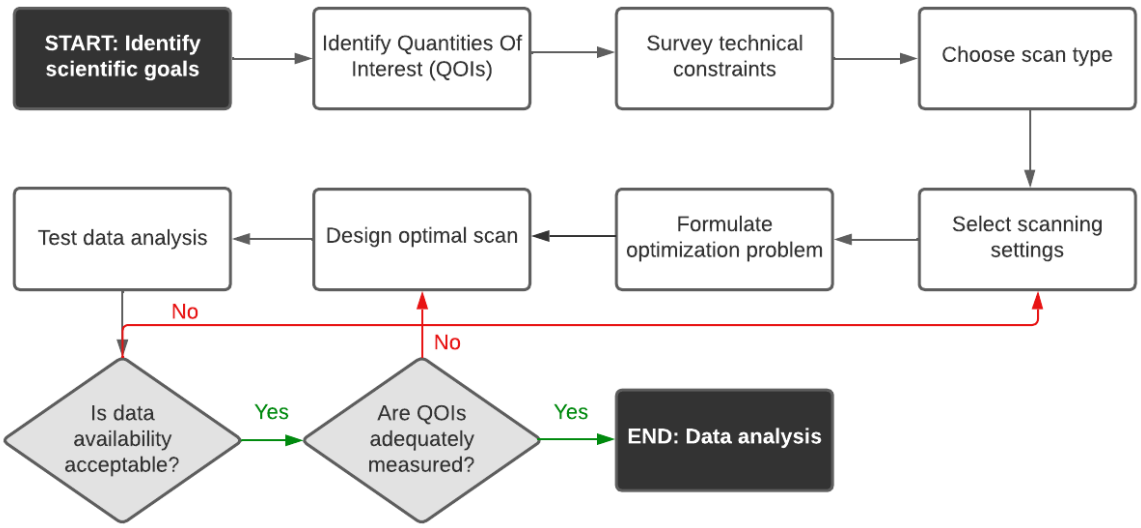

Figure 1. Workflow of the scan design process.

2.1. Identifying the quantities of interest

As a preliminary step, the generic scientific goals of the field campaign are translated into quantities of interest (QOI), namely the measurands to be experimentally observed to address the specific needs of the project, usually represented by the instantaneous wind velocity components ("turbulence", hereinafter) and their statistics. The user also needs to define the spatio-temporal resolution of the QOI, quantitatively evaluated in terms of the cut-off spatial (half) wavelengths, here indicated by the three-dimensional (3D) vector, $\mathbf{\Delta n_0} = [\Delta n_{0,x}, \Delta n_{0,y}, \Delta n_{0,z}]$, (streamwise,

spanwise, and ground-normal directions, respectively) in accordance with LiSBOA [11], and the energetic content in the temporal domain, characterized by the power spectral density, $\phi_u(f)$.

2.2. Technical constraints

The technical constraints of a lidar field campaign are generally connected to the allowable deployment locations of lidars, the obstructions blocking the line of sight, the maximum range of the lidar as a function of the operative parameters, and the sampling time as a function of the scan parameters. While the first two are known a priori based on the site layout, the latter are instrument-specific and, in the case of the maximum range, also dependent upon the atmospheric conditions.

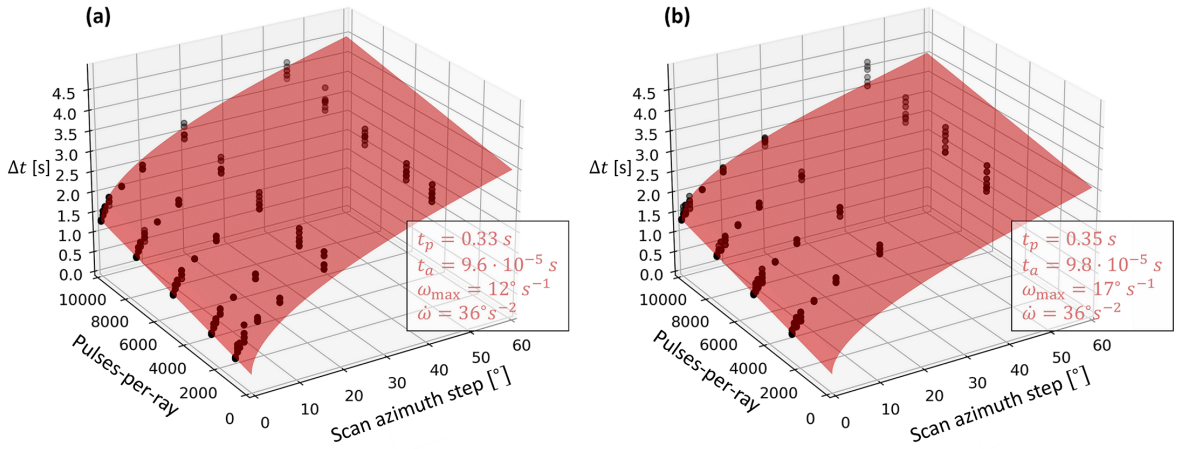

Figure 2. Parametric estimation of the sampling time of (a) customized Halo XR and (b) Halo XR+. The black dots represent lidar data while the red surface is the model based on the fitted Eq. 1.

The lidar sampling time, Δt, is not a constant value, and a simple model to describe it can be formulated considering the lidar acquisition process and the kinematic of the scanning head:

$$\Delta t = t_p + \mathrm{PPR} \cdot t_a + t_m \tag{1}$$

where t_p is the processing time, t_a is the time required for acquiring the backscattering signal from a single pulse, PPR is the lidar pulses per ray. The scan moving time, t_m, is calculated by integrating the law of motion of the scanning head that travels from θ to $\theta + \Delta\theta$ with a constant angular acceleration, $\dot{\omega}$, and up to a maximum angular speed, $\omega_{\max}$:

$$t_m = \begin{cases} \sqrt{\frac{2\Delta\theta}{\dot{\omega}}} & \text{if } \Delta\theta \leq \frac{\omega_{\max}^2}{2\dot{\omega}} \\ \frac{\omega_{\max}}{2\dot{\omega}} + \frac{\Delta\theta}{\omega_{\max}} & \text{if } \Delta\theta > \frac{\omega_{\max}^2}{2\dot{\omega}}, \end{cases} \tag{2}$$

In Fig. 2 we show examples of how the lidar sampling time varies as a function of PPR and $\Delta\theta$ for the two commercial lidar models we use in our analysis. For the two lidar types used in our field experiments, we estimated all the parameters of equations 1 and 2 by performing a least-square fitting to the results of a dedicated field test comprising multiple plan-position-indicator (PPI) scans at different PPRs and $\Delta\theta$ (see Figure 2).

2.3. Choosing the scan type

The knowledge of the QOI and constraints is generally sufficient to select the type of scan that meets the scientific goals of the projects. Typical scanning patterns are stare scans [13], which are generally used to acquire line-of-sight (LOS) velocity scanning at the highest possible sampling speed; PPI scans [8], wherein an azimuth range at a constant elevation angle is scanned; range-height-indicator (RHI) scans [14], which are useful to characterize the vertical profile of LOS velocity; volumetric scans [15], wherein a 3D volume is probed with a sequence of PPIs or RHIs; and profiling scans [16], like the Doppler-beam swinging (DBS) and the Velocity-Azimuth Display (VAD), which leverage the assumption of horizontal homogeneity to reconstruct the vertical profile of the wind components.

2.4. Selecting the scanning settings

The main scanning settings that can be selected a priori are the range gate length, Δr, and the PPR. In our case, those parameters were set to reasonable values based on previous campaigns, thereby representing a trade-off between maximum range and spatial resolution (inversely proportional to Δr) and scanning time (proportional to PPR, see equation 1). These parameters will eventually be increased (decreased) if the data availability during the campaign turns out to be too low (high enough to allow for faster sampling).

2.5. Formulating the scan optimization problem

Once the former scanning settings are fixed, the main task for the lidar scan designer is to define the geometry of the scan, which is a function of the azimuth resolution, $\Delta\theta$, and span, $\theta_{\max}$ (PPI and volumetric scans), and elevation resolution, $\Delta\beta$, and span, $\beta_{\max}$ (RHI and volumetric scans). These parameters are chosen based on a trade-off between the spatial and temporal resolution. In other words, given a scanning mode, there is a combination of parameters that provides the best spatio-temporal characterization of the turbulent field under investigation. As a general principle, wide scans with fine angular steps and, therefore, a long sampling time, maximize spatial resolution, whereas narrow and coarse scans achieve a higher statistical significance and capture faster eddies.

The original LiSBOA tool defines a mathematical framework to quantify the performance of a scan setting to reconstruct the spatial variability of flow statistics in terms of two objective functions to be minimized:

- ϵ^I, the ratio of undersampled volume, defined as the fraction of the volume of interest in which the smaller spatial mode of interest (fundamental mode, hereinafter) is not adequately sampled, is a metric quantifying the spatial resolution. The fundamental mode is characterized in the spectral domain by the fundamental half wavelength, $\mathbf{\Delta n_0}$
- ϵ^{II}, the error on the mean, is the statistical uncertainty of the mean of the sampled LOS velocity, which is a function of the integral timescale and the number of repetitions of the scan. In this context, the ϵ^{II} is normalized by the local standard deviation of the velocity.

It is noteworthy that the term "statistics" in this work refers essentially to mean, variance (or spectra) of the streamwise velocity, although only the uncertainty on the former is used in the scan design phase for the sake of simplicity. The original framework is here enhanced with the introduction of a third objective function, defined as the ratio of unresolved energy, namely the fraction of the energy content of the LOS velocity signal residing at frequencies higher than the Nyquist frequency associated with the sampling time of the lidar. Formally:

$$\epsilon^{III} = \frac{1}{\langle u'^2 \rangle} \int_{\frac{1}{2\tau_s}}^{\infty} \phi_u(f) df, \tag{3}$$

where $\langle u'^2 \rangle$ is the streamwise velocity variance and τ_s is the sampling time of one scan. This approach relies on the assumption (which is applied hereinafter) that the flow is fairly aligned (within $\sim 20 - 30°$) with the lidar beam, which helps leverage the LOS velocity de-projection to estimate u [8]. This simplification thereby approximates the first- and second-order statistics of the streamwise component with that of the horizontal-equivalent velocity.

2.6. Designing the optimal scan

To apply the theory described in Section 2.5, users must choose the optimal scan geometry by using a graphical tool in the form of a Pareto front. Figure 3 shows a conceptual 3D Pareto front

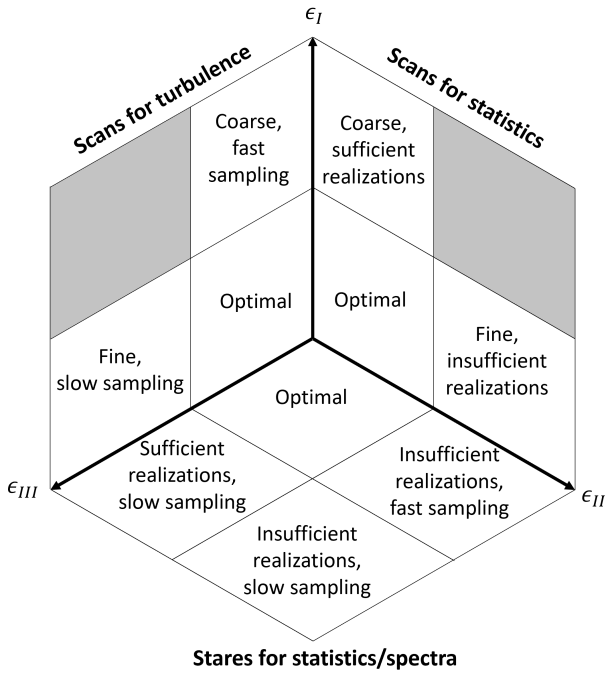

Figure 3. The 3D optimization space of the scan design. Specific applications of these scanning approaches for RAAW and AWAKEN are described in Sections 3 and 4.

to illustrate the possible scenarios. Based on the specific goals of the experiment, the designer may consider just a subset of the objective functions. Focusing on ϵ^I and ϵ^{II} only, for instance, is suitable to design scans that aim to derive flow statistics; ϵ^I and ϵ^{III} guide the optimization of scans targeting time-evolving turbulent fields; ϵ^{II} and ϵ^{III} can help identify optimal stare modes, wherein the spatial resolution is of secondary importance. Thus, in practice, a two-dimensional (2D) Pareto front will suffice to identify the best set of angular steps and ranges for a given type of scan.

2.7. Testing data analysis

After identifying the optimal scan, it is common practice to run the lidar for a few realizations to calculate preliminary QOI to assess the goodness of the designed scan. If there are unsatisfactory results in terms of data availability, the lidar settings may need to be adjusted. If, conversely, the flow reconstruction is flawed in spite of the raw data quality, the scan optimization process needs to be revised with a more careful definition of the optimization problem. In fact, the proposed approach relies on a priori estimation of the turbulent flow spatio-temporal structure,

the lidar performance, and the duration of the experiment, which are not always known with a high level of certainty.

3. Application 1: the RAAW field campaign

3.1. Overview

The RAAW experiment is a unique collaboration between research institutions and the private sector to create validation benchmarks for improving numerical simulation of wind turbine aerodynamics, characterizing advanced turbine operation, and studying inflow and wake physics. The RAAW field campaign is taking place in Lubbock, Texas, at a General Electric (GE) research facility where one 2.8-MW, 120-m hub height (H), 127-m rotor diameter (D) wind turbine is located. The RAAW turbine was instrumented in summer 2022 with two nacelle-mounted Halo Streamline XR scanning lidars, one for characterizing the inflow, and the other for observing turbine wakes. In early 2023, a forward-facing spinner lidar [17] was installed on the wind turbine's hub. Several other remote-sensing and in situ instruments were also deployed to thoroughly characterize the inflow. The wind turbine is equipped with load sensors and blade deflection and torsion are measured via a photogrammetry system. The instruments are expected to remain deployed until fall 2023. Observations will help address the project science goals in the following areas:

- Inflow and wake science, which include a comprehensive spatio-temporal characterization of inflow and mean and dynamic near-to-far wake to quantify a variety of phenomena, including the effects of axial induction control on the wake, wake dynamics, flow spatial coherence, and turbulence dissipation rates.
- Wind turbine science, which includes quantifying aerodynamic loads and characterizing wind turbine response under off-normal operating conditions.
- Across-scale model validation, which includes time series validation of inflow, wind turbine response and wake, statistical validation of inflow and wind turbine response, and uncertainty quantification of measured signals.

3.2. Scanning strategy

The scanning strategy is tailored to target the quantities of interest of RAAW, namely the morphology and dynamics of the incoming turbulent eddies interacting with the wind turbine, the wake dynamics, and the first- and second-order statistics of the inflow and wake. The process follows the schematic in Fig. 3.

A survey of the research goals narrowed down the set of QOI to the streamwise velocity, $u(x, y, z, t)$, and its first- and second-order moments, $\langle u \rangle(x, y, z)$ and $\langle u'^2 \rangle(x, y, z)$, with a spatio-temporal resolution to solve eddies and flow structures relevant for the study of the turbine operation. Ancillary quantities are the wind profile above the turbine and the spanwise velocity at hub height, $v(0, y, H, t)$, which are useful to study lateral coherence and wake meandering. Therefore, we conducted separate optimizations for scans measuring turbulence and statistical reconstruction of the flow.

Next, we quantified the severity of the LOS blockage due to the turbine components by performing a hard target test by swiping the full scanning volume and recording the signal-to-noise ratio (SNR), as reported in Fig. 4. The inflow lidar is blocked (i.e., low SNR values) by the nacelle roof and hub for all negative elevations, whereas the wake lidar has a clear line of sight for elevation as low as $\beta = -30°$ scanning downstream. Blades (that were parked during this test) also represent a major and unavoidable source of data loss upstream.

The knowledge of the QOI and technical constraints suffices to identify the allowable scanning sequence, which is summarized in Table 1. The sequence includes 15-minute fast PPIs probing the time-varying turbulent inflow and wake fields followed by 10-minute scans targeted at

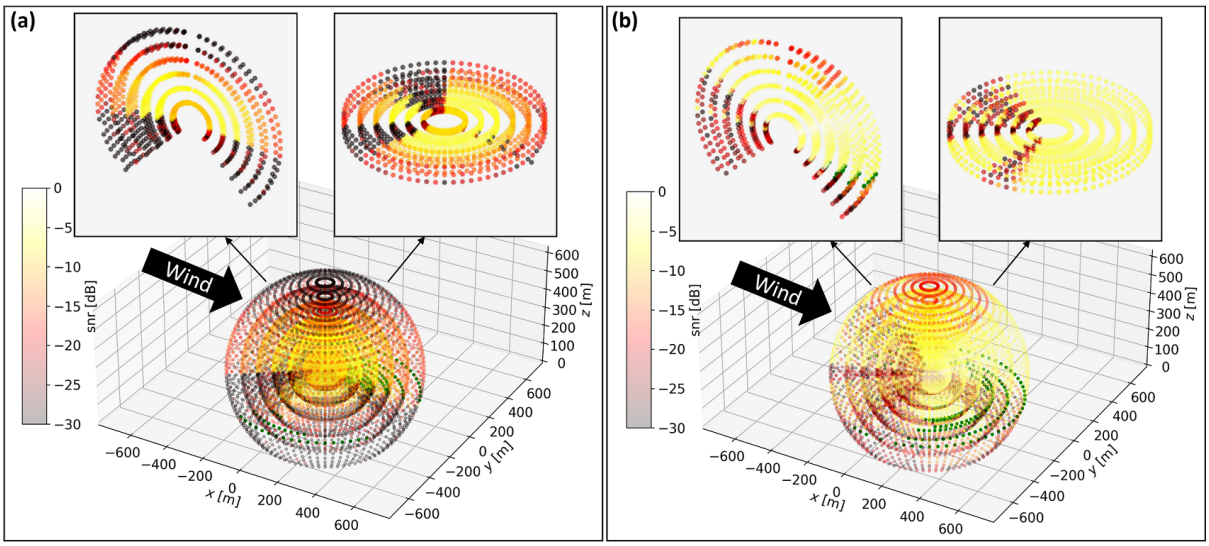

Figure 4. Spatial distribution of SNR resulting from a hard target test performed with the (a) inflow and (b) wake nacelle-mounted lidars at RAAW. Data along the wind turbine axis (left cutout) and at hub height (right cutout) are extracted for clarity. The green dots represent the backscattering from the ground.

assessing flow statistics. The horizontal homogeneity of the incoming flow allows using coarse staring beams for characterizing $\langle u \rangle$, $\langle u'^2 \rangle$, and even spectra, whereas the inherently 3D wake flow is probed in a volumetric fashion. Auxiliary scans, such as DBS, and lateral and wake stares are also scheduled. The whole sequence lasts 30 minutes, which falls within the spectral gap of atmospheric turbulence where the mesoscale forcing can oftentimes be assumed as steady [18].

Table 1. Scan Sequence for the RAAW Nacelle-Mounted Lidars.

Inflow lidar				**Wake lidar**			
Scan name	**Type**	**Time**	**QOI**	**Scan name**	**Type**	**Time**	**QOI**
Turbulence	PPI	15 min	$u(x,y,H,t)$	Turbulence	PPI	15 min	$u(x,y,H,t)$
DBS	Profiling	0.5 min	$\mathbf{u}(z)$	Statistics	Volumetric	10 min	$\langle u \rangle(x,y,z)$ $\langle u'^2 \rangle(x,y,z)$
Statistics	Multi-stare	9.5 min	$\langle u \rangle(x,0,H)$ $\langle u'^2 \rangle(x,0,H)$ $\langle \theta_w \rangle(H)$				
Lateral stare	Stare	4.5 min	$v(0,y,H,t)$	Wake stare	Stare	5 min	$u(x,0,H,t)$
DBS	Profiling	0.5 min	$\mathbf{u}(z)$				

The pulses per ray are set to PPR $= 1,000$ to minimize the acquisition time, and we choose the minimum allowable range gate length of $\Delta r = 12$ m. The associated expected range under favorable weather conditions is 1,500 m ($\sim 12D$).

Next, the scans for turbulence and statistics are optimized using the enhanced LiSBOA framework. A domain extending $x = \pm 10D, y = \pm 2D, z = \pm 1D$ is considered. Other LiSBOA settings are those recommended in [11]. The optimal geometrical parameters for the scans in Table 1 include:

- **Inflow and wake turbulence.** This scan targets fundamental modes with half wavelength $\mathbf{\Delta n_0} = [1, 0.25]D$ on the hub-height plane, whereas the distribution of energy across temporal scales is approximated by the Kaimal spectrum for a hub-height wind speed of

$U_\infty = 10$ m s^{-1} [19] (other wind speeds have been tested but did not affect the optimal scan selection). The optimization is carried out considering the $\epsilon^I - \epsilon^{III}$ Pareto front, which is shown in Fig. 5a. Out of the points lying on the optimal frontiers (i.e., the bottom-left edge of the cloud), we selected $\Delta\theta = 2°$ and $\theta_{\max} = 15°$. This scan takes 16 seconds to complete and has a data loss of $\epsilon^I \sim 38\%$ (i.e., the fundamental mode is well-sampled in most of the domain shown in the figure) and does not solve $\epsilon^{III} \sim 27\%$ of the temporal scales. These values have been deemed acceptable for data assimilation with the high-fidelity model used in this project. It is noteworthy that the same scan design is also applied to the wake lidar for consistency, although we are aware that the presence of the rotor is expected to change the spectrum of u [20]. The field data from the nearby instrumented meteorological tower will allow to assess the accuracy on the lidar-based inflow and wake statistics for selected wind directions.

- **Inflow statistics.** This scan includes N_θ symmetric beams at hub height and is mostly driven by the ϵ^{III} value, which is relevant to quantify the inaccuracy of the spectral quantities. In fact, the error on the mean, ϵ^{II}, varies less than 2% for all the tested conditions due to the large number of realizations, and ϵ^I is not applicable. Figures 5b-d report ϵ^{III} for different N_θ, $\theta_{\max}$, and U_∞. $N_\theta = 3$ and $\theta_{\max} = 20°$ was selected due to the limited unresolved energy ($\epsilon^{III} < 20\%$) for all wind speeds and it is wide enough to allow for an estimation of the mean wind direction [21].
- **Wake statistics.** The optimization of the volumetric scan follows the procedure outlined in [11], being a mere application of the original LiSBOA algorithm. The best volumetric scan has an opening angle of $\theta_{\max} = \beta_{\max} = 15°$ and an angular resolution of $\Delta\theta = \Delta\beta = 3°$ (Fig. 5e), which agrees with previous simulation studies [10].

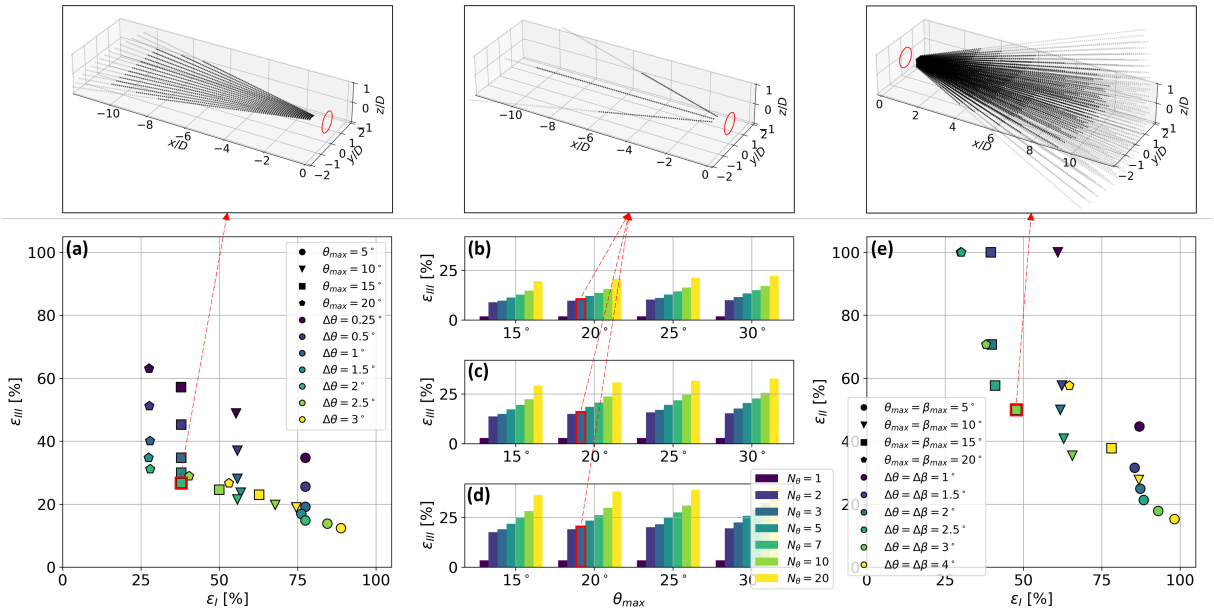

Figure 5. Summary of the scan optimization results for RAAW: (a) fast PPI for turbulence; (b-d) multi-stare for inflow statistics for $U_\infty = 5$, 10, and 15 m s^{-1}, respectively; (e) volumetric wake scan for statistics. The optimal scan geometry is blown up in the top panels. Points that are greyed out are outside of the domain of interest.

4. Application 2: the AWAKEN field campaign

4.1. Overview

The AWAKEN field campaign brings together multiple research institutions and private companies to assess wind farm-atmosphere interactions and test advanced wind power plant control strategies, such as wake steering. AWAKEN is taking place in Northern Oklahoma, in a region where nearly 1,000 wind turbines are located within a 50-km radius of the U.S. Department of Energy's Atmospheric Radiation Measurement program's Central Facility, a long-term atmospheric observatory. Observations will be collected from 13 field sites and four instrumented wind turbines within the King Plains wind plant (Figure 6). While the field sites were instrumented throughout fall 2022, the wind turbines will be instrumented in early 2023.

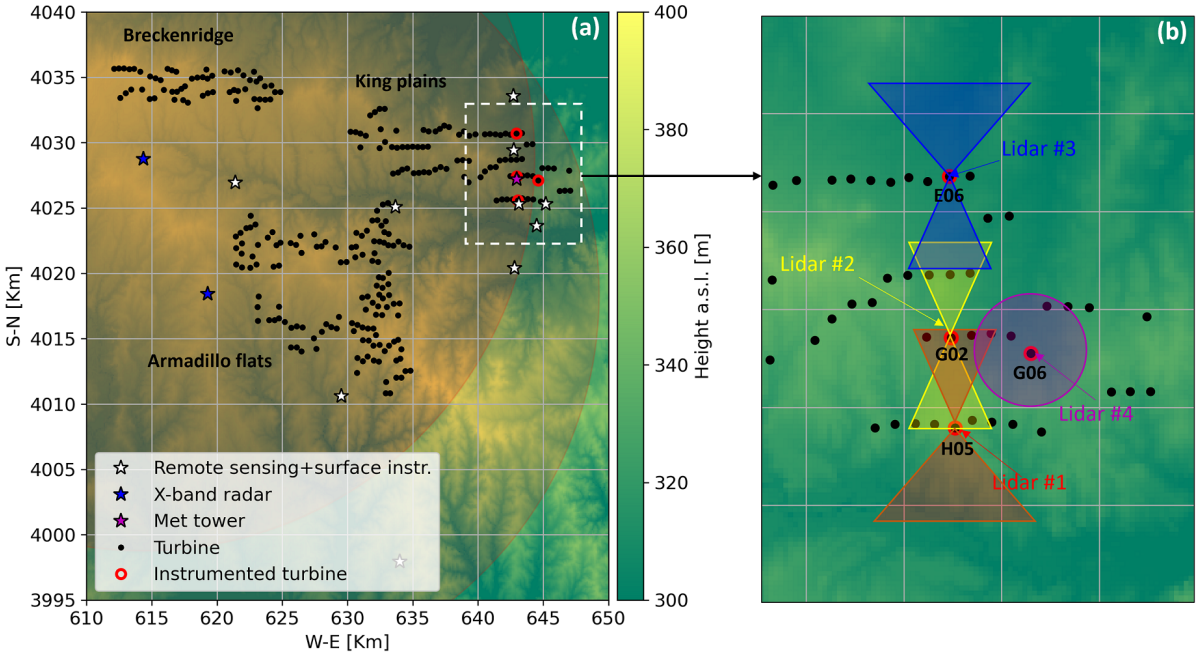

Figure 6. Layout of the AWAKEN site: (a) top view of all of the experimental sites; (b) zoomed-in map of the instrumented wind turbines and nacelle-mounted scanning lidars.

Among other instruments, all four turbines (GE 2.82-MW machines, with a $\sim$ 89-m hub height and 127-m rotor diameter) will have nacelle-mounted lidars, whose observations will be leveraged to characterize inflow and turbine wakes to help address five of the project's testable hypotheses. A detailed description of the hypotheses can be found in [22]. More broadly, the scanning lidar measurements will be leveraged to characterize the wind turbine and wind plant wakes, wind plant blockage, turbulence levels within wind plants, and for wake steering experiments.

As detailed in [23], the dominant wind direction at the site is from the south, meaning that turbine H05 in Fig. 6 will typically be the upwind instrumented wind turbine, whereas E06 will be the downwind one. Each turbine will have one nacelle-mounted Halo Streamline XR/XR+ scanning lidar, and the southernmost turbine will be equipped with a Windcube nacelle lidar.

4.2. Scanning strategy at the AWAKEN field campaign

The AWAKEN field has a similarly broad set of QOI as RAAW that requires specialized scans to address turbulence and statistics separately. However, the additional interest in the flow at

Table 2. Scan Sequence for the AWAKEN Nacelle-Mounted Lidars #1, #2, and #3. *The farm statistics scan is different for each lidar (see Section 4.2).

Scan Name	Wake Steering	Type	Time	QOI
Inflow turbulence	off	PPI	30 min	$u(x, y, H, t)$
Wake meandering	off	PPI+RHI	30 min	$u(x, y, H, t)$ $u(x, 0, z, t)$
Inflow statistics/turbulence (wide)	on	PPI	20 min	$u(x, y, H, t)$ $\langle u \rangle(x, y, H)$ $\langle u'^2 \rangle(x, y, H)$ $\langle \theta_w \rangle(H)$
Wake 2D statistics (wide)	on	PPI	20 min	$\langle u \rangle(x, y, H)$ $\langle u'^2 \rangle(x, y, H)$
Wake 3D statistics (wide)	on	Volumetric	20 min	$\langle u \rangle(x, y, z)$ $\langle u'^2 \rangle(x, y, z)$
Inflow statistics	off	PPI	20 min	$\langle u \rangle(x, y, H)$ $\langle u'^2 \rangle(x, y, H)$ $\langle \theta_w \rangle(H)$
Wake 3D statistics	off	Volumetric	20 min	$\langle u \rangle(x, y, z)$ $\langle u'^2 \rangle(x, y, z)$
Farm statistics*	off	Volumetric	20 min	$\langle u \rangle(x, y, z)$ $\langle u'^2 \rangle(x, y, z)$

the wind plant scale and an active wake steering scheme implemented at the wind plant require an even more diversified sequence of scans.

Active wake steering introduces an intentional yaw offset of the wind turbine to deflect the wake away from downstream turbines and increase overall wind plant production. The magnitude and direction of the applied yaw offset depend on the flow conditions and are not known beforehand. Therefore, the azimuth range of the scans implemented on the Doppler lidars while wake steering is active needs to be broadened to capture the wake (or the incoming wind field) under yawed conditions. Broadening scan sectors makes scans targeted at instantaneous turbulence challenging during periods with active wake steering due to the excessive sampling time.

These considerations contributed to the creation of the scan sequence described in Table 2, in which scans during baseline control (i.e., when wake steering is off) switch to wider scans when the yaw is intentionally misaligned. As for RAAW, faster scans are devoted to detecting the turbulent field, whereas slower scans are used to reconstruct flow statistics. Unlike RAAW, however, in AWAKEN the inflow is often affected by upstream wakes that induce a spatial inhomogeneity, thereby preventing the use of multi-stare scans. Synchronized scheduling of the scan sequence across all lidars will provide the QOI across multiple turbine rows of the wind farm simultaneously. The specific properties of each optimal scan identified through the enhanced LiSBOA process and based on Table 2 are listed in the following bullets. The following parameters apply to lidars #1, #2, and #3 unless otherwise specified, with lidar #4, which focuses on detecting speedups, being treated separately:

- **Inflow turbulence.** This upstream PPI scan samples the time-varying incoming flow at hub height to analyze the wind turbine loads and performance (Fig. 7a). It has an opening angle of $\theta_{max} = 15°$ and an azimuth step of $\Delta\theta = 1.5°$ based on $\mathbf{\Delta n_0} = [1, 0.25]D$. This setup provides 20 data points across the scanning area every 22 seconds.
- **Wake meandering.** This cross-shaped scan captures a vertical and horizontal cross section of the wake to investigate wake meandering (Fig. 7b). Resolving turbulence scales larger

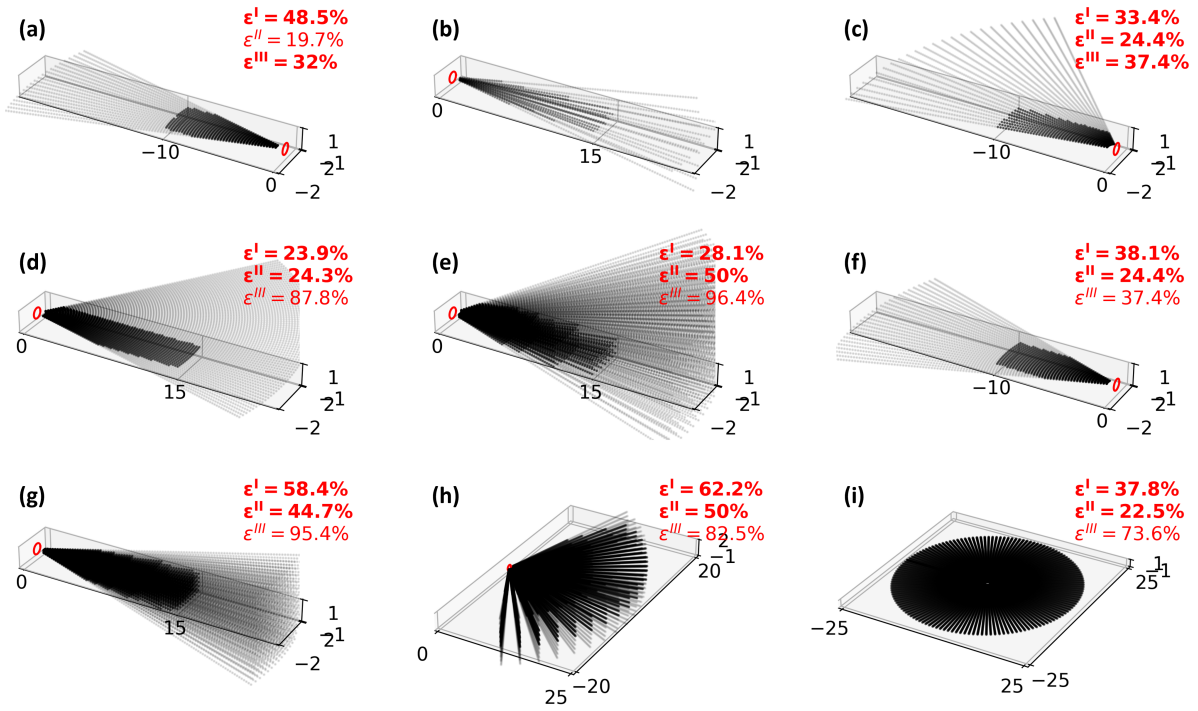

Figure 7. Optimal scanning patterns for AWAKEN: (a) inflow dynamics; (b) wake meandering; (c) inflow statistics/dynamics (wide); (d) wake 2D statistics (wide); (e) wake 3D statistics (wide); (f) inflow statistics; (g) wake 3D statistics; (h) farm statistics; (i) speedup. The bold quantities represent the relevant objective functions used for the optimization. The spatial unit is D and points that are greyed out are outside of the domain of interest.

than $2D$, which are assumed to drive wake meandering, for wind speeds up to 14 m s^{-1} requires that the scan is completed in 10 s based on the Nyquist-Shannon sampling theorem [24]. This is achieved with the continuous-scan mode of the Doppler lidars using an opening angle of $\pm 10°$ and an angular resolution of 3° for both azimuth and elevation.

- **Inflow statistics/turbulence (wide).** An upstream scan through the rotor with a wide opening angle of $\theta_{max} = 30°$ to capture inflow statistics and dynamics as small as half of the rotor scale (i.e., $\mathbf{\Delta n_0} = [1, 0.5]D$) during active wake-steering events (Fig. 7c). In addition to inflow statistics, this scan can also provide a redundant estimation of the true yaw angle. A simultaneous optimization of ϵ^I, ϵ^{II}, and ϵ^{III} led to the choice of $\Delta\theta = 2.5°$, resulting in a temporal resolution of approximately 30 s.
- **Wake 2D statistics (wide).** A horizontal cross section with a wide opening angle to capture wake statistics even if the wind turbine is operating with a yaw offset of $\pm 20°$ (Fig. 7d). The scan is a horizontal PPI in the downstream direction with an opening angle of $\theta_{\max} = 35°$ centered on the rotor axis and an azimuth step of $\Delta\theta = 1.0°$ and takes ~ 70 s to complete with 16 repetitions within a 20-minute time slot. The small fundamental half wavelength $\mathbf{\Delta n_0} = [1, 0.25]D$ and the large downstream domain extent ($15D$) allow to finely solve the hub-height flow down to the following array of wind turbines at King Plains.
- **Wake 3D statistics (wide).** This scan consists of multiple, vertically stacked PPIs providing a volumetric view of the wake up to $15D$ downstream (Fig. 7e). The required spatial resolution is relaxed compared to the RAAW counterpart ($\mathbf{\Delta n_0} = [1, 1, 1]D$) due to the larger scanning volume. The optimal scan has an angular resolution of 2.5° for both

azimuth and elevation angle with $\theta_{\max} = 30°$ and $\beta_{\max} = 10°$ to take into account yaw misalignment.

- **Inflow statistics.** This PPI with $\theta_{\max} = 20°$ and $\Delta\theta = 1.5°$ represents the best setup to solve relevant incoming atmospheric eddies and wake-generated turbulent structures and uses $\mathbf{\Delta n_0} = [1, 0.25]D$ (Fig 7f).
- **Wake 3D statistics.** It has a similar design to the wide 3D statistic scan, but without wake steering it can use a smaller opening angle of $\pm 10°$ and higher angular resolution of 1.5° for both azimuth and elevation (Fig 7g). The spatial resolution is $\mathbf{\Delta n_0} = [1, 0.5, 0.5]D$, which should resolve the wake shape up to $15D$ downstream, resulting in a thorough characterization of the wake morphology under different inflow conditions.
- **Farm statistics.** The scans targeted at the wind farm statistic will be implemented only at lidars #1 and #3, whereas lidar #2 keeps executing 3D statistics scans. The farm statistics scan samples of the 3D flow field upstream (lidar #1) and downstream (lidar #3) to statistically characterize the blockage and farm wake, respectively. It solves large flow features ($\mathbf{\Delta n_0} = [5, 5, 1]D$) up to the maximum lidar range and uses $\theta_{max} = 60°$, $\beta_{max} = 10°$, $\Delta\theta = 7.5°$, and $\Delta\beta = 2°$ (Fig 7h). The 3D nature of blockage for this specific site is analyzed by [6].
- **Speedup.** Lidar #4, which is located east of the main transect (Fig. 6b) performs a 360-degree PPI to monitor the hub-height flow searching for pressure-induced speedups and channeling effects (Fig 7i). The azimuth resolution is $\Delta\theta = 2.5°$ and should solve modes greater than $\mathbf{\Delta n_0} = [5, 5, 1]D$ in most of its range.

It is worth emphasizing that the present setup may undergo future adjustments during the campaign, in particular regarding the scanning mode (step stare vs. continuous) and the PPR and gate length values used.

5. Conclusions

This work offers a pragmatic and actionable experimental design study for lidar scan optimization. The optimal design minimizes the spatial and temporal undersampling and statistical uncertainty of the quantities of interest based on a-priori information of the flow, whereas a comparison with redundant in-situ measurements will allow to quantify the uncertainty in real-world conditions. The relevance of the methodological approach presented here goes beyond the RAAW and AWAKEN field experiments, because the proposed pipeline takes into account the specific capabilities of commercial scanning lidar systems, line-of-sight blockage, and real-world flow scenarios so that it can be applied to future field deployments, both onshore and offshore. This study also emphasizes the novel opportunities and additional complexity introduced by remote-sensing technology and the substantial preparatory work necessary to leverage its full potential.

Acknowledgments

This work was authored in part by the National Renewable Energy Laboratory, operated by Alliance for Sustainable Energy, LLC, for the U.S. Department of Energy (DOE) under Contract No. DE-AC36-08GO28308. Funding provided by the U.S. Department of Energy Office of Energy Efficiency and Renewable Energy Wind Energy Technologies Office. The views expressed in the article do not necessarily represent the views of the DOE or the U.S. Government. The U.S. Government retains and the publisher, by accepting the article for publication, acknowledges that the U.S. Government retains a nonexclusive, paid-up, irrevocable, worldwide license to publish or reproduce the published form of this work, or allow others to do so, for U.S. Government purposes. This research was funded in part by the Swiss Federal Office of Energy (Grant Number SI/502135-01).

References

[1] Barthelmie R, Pryor S, Frandsen S, Hansen K, Schepers J, Rados K, Schelz W, Neubert A, Jensen L and Neckelmann S 2010 *J. Atmos. Ocean. Technol.* 1302–1317
[2] Letizia S and Iungo G V 2022 *Journal of Renewable and Sustainable Energy* **023301**
[3] Lundquist J, DuVivier K, Kaffine D and Tomaszewski J 2019 *Nat Energy* **4** 26–34 ISSN 2058-7546 URL http://dx.doi.org/10.1038/s41560-018-0281-2
[4] Nygaard N G, Steen S T, Poulsen L and Pedersen J G 2020 *Journal of Physics: Conference Series* **1618** ISSN 17426596
[5] Schneemann J, Theuer F, Rott A, Dörenkämper M and Kühn M 2021 *Wind Energy Science* **6** 521–538 ISSN 23667451
[6] Sanchez Gomez M, Lundquist J K, Mirocha J D, Arthur R S, Muñoz-Esparza D and Robey R 2022 *Journal of Renewable and Sustainable Energy* **14** 063303 publisher: American Institute of Physics URL https://aip.scitation.org/doi/10.1063/5.0103668
[7] Liu Z, Barlow J F, Chan P W, Fung J C H, Li Y, Ren C, Mak H W L and Ng E 2019 *Remote Sensing* **11** 1–47 ISSN 20724292
[8] Zhan L, Letizia S and Valerio Iungo G 2020 *Wind Energy* **23** 501–527
[9] Krishnamurthy R, Choukulkar A, Calhoun R, Fine J, Oliver A and Barr K 2013 *Wind Energy* **16** 189–206
[10] Carbajo Fuertes F, Markfort C D and Porté-Agel F 2018 *Remote Sens.* **10** 668
[11] Letizia S, Zhan L and Valerio Iungo G 2021 *Atmospheric Measurement Techniques* **14** 2095–2113 ISSN 23318422
[12] Letizia S, Zhan L and Valerio Iungo G 2021 *Atmospheric Measurement Techniques* **14** 2065–2093
[13] Puccioni M and Valerio Iungo G 2021 *Atmospheric Measurement Techniques* **14** 1457–1474 ISSN 18678548
[14] Banta R, Yelena L and Brewer W 2006 *Journal of Atmospheric Sciences* **63** 2700–2719
[15] Iungo G V and Porté-Agel F 2014 *Journal of Atmospheric and Oceanic Technology* **31** 2035–2048
[16] Sathe A, Mann J, Vasiljevic N and Lea G 2015 *Atmospheric Measurement Techniques* **8** 729–740 ISSN 18678548
[17] Mikkelsen T, Angelou N, Hansen K, Sjöholm M, Harris M, Slinger C, Hadley P, Scullion R, Ellis G and Vives G 2013 *Wind Energy* **16** 625–643 ISSN 10954244
[18] Burton T, Jenkins N an Sharpe D and Bossanyi E 2001 *Wind Energy Handbook* (Wiley) pp 9–38
[19] International Electrotechnical Commision 2005 IEC 61400-1 Tech. Rep. 2 International Electrotechnical Commision
[20] Chamorro L P, Guala M, Arndt R E and Sotiropoulos F 2012 *J. of Turbul.* **13** 1–13 ISSN 14685248
[21] Kragh K A, Hansen M H and Mikkelsen T 2013 *Wind Energy* **16** 353–366 ISSN 10954244
[22] Moriarty P, Bodini N, Brugger P, Goldberger L, Hamilton N, Herges T, Hirth B, Iungo G V, Ivanov H, Kaul C, Klein P, Krishnamurthy R, Letizia S, Lundquist J K, Morris V R, Newsom R, Pekour M, Porté-Angel F, Scholbrock A, Schroeder J, Simley E, Wharton S and Zalkind D *Submitted to Journal of Renewable and Sustanaible Energy*
[23] Turner D and Ellingson R 2017 *The Atmospheric Radiation Measurement (ARM) Program: The First 20 Years* (American Meteorological Society)
[24] Reinwardt I, Schilling L, Dalhoff P, Steudel D and Breuer M 2020 *Wind Energy Science* **5** 775–792 URL https://wes.copernicus.org/articles/5/775/2020/